Investigation of phenomenological models for the Monte Carlo simulation of the prompt fission neutron and γ emission

O. Litaize and O. Serot
CEA Cadarache, F-13108 Saint Paul lez Durance, France
(Received 19 July 2010; published 29 November 2010)

A Monte Carlo simulation of the fission fragment deexcitation process was developed in order to analyze and predict postfission-related nuclear data which are of crucial importance for basic and applied nuclear physics. The basic ideas of such a simulation were already developed in the past. In the present work, a refined model is proposed in order to make a reliable description of the distributions related to fission fragments as well as to prompt neutron and γ energies and multiplicities. This refined model is mainly based on a mass-dependent temperature ratio law used for the initial excitation energy partition of the fission fragments and a spin-dependent excitation energy limit for neutron emission. These phenomenological improvements allow us to reproduce with a good agreement the ^{252}Cf(sf) experimental data on prompt fission neutron multiplicity $\overline{\nu}(A)$, $\overline{\nu}(TKE)$, the neutron multiplicity distribution $P(\nu)$, as well as their energy spectra $N(E)$, and lastly the energy release in fission.

DOI: 10.1103/PhysRevC.82.054616 PACS number(s): 24.75.+i, 24.10.Lx, 24.60.Dr, 21.10.Ma

I. INTRODUCTION

The data related to fission fragments (FF) are of crucial importance for applied and basic nuclear physics. Their kinetic and excitation energies at scission and after full acceleration are at the root of the prompt neutron and γ emission. Spectra and multiplicities of prompt particles are as important as cross sections since the energies released during fission by FF and prompt particles are directly related to the heat deposited in nuclear reactors.

Among the fission observables, the prompt fission neutron spectra and average multiplicities are commonly described by the Madland-Nix Los Alamos model [1]. This model was refined in order to account for the fission fragment mass, charge, and kinetic energy distributions [2] and applied by Vladuca and Tudora in their so-called point-by-point model [3,4] by considering, among other things, fission modes.

In order to predict and analyze the various neutron, γ, and fission-fragment-related data, a Monte Carlo approach simulating the FF deexcitation was undertaken by Lemaire *et al.* [5] and very recently by Randrup and Vogt in Refs. [6,7]. In Lemaire's work, two kinds of hypotheses related to the partitioning of the FF initial excitation energy at the scission point were considered. The first one is an equipartition of the temperature between the two complementary fragments and the second one uses experimental results, such as mean neutron energy or the average number of prompt neutrons, as a function of the fission fragment mass to infer the initial excitation energy of each fragment. The first hypothesis is not able to reproduce the sawtooth shape of the distribution of the average number of prompt neutrons as a function of the fragment mass and the second one is not a predictive calculation route due to experimental results used as input parameters.

In the present work, a dedicated Monte Carlo code named FIFRELIN (fission fragment evaporation leading to an investigation of nuclear data) was developed, including various improved models mainly based on a mass-dependent temperature ratio of the fully accelerated complementary fragments and a spin-dependent excitation energy limit for neutron emission to improve the agreement with experimental data.

Section II details the method and models implemented in our Monte Carlo code while Sec. III is devoted to the analysis of the different models in comparison with selected experiments from literature. The data presented in this paper are related to the ^{252}Cf spontaneous fission.

II. MODEL DESCRIPTION

As usual a Monte Carlo game can only be performed with the knowledge of physical probability density functions through the repartition functions. The most basic probability laws concern the mass and the kinetic energy of the fission fragments. These are experimental distributions. Another distribution needed to select a nucleus (a fission fragment) concerns the nuclear charge (Z). The next step in the simulation consists of calculating the excitation energy. The total excitation energy (TXE) at scission is composed of intrinsic excitation energy $E^{*,\mathrm{sc}}$, deformation energy $E^{\mathrm{def,sc}}$, and rotational energy

$$\mathrm{TXE} = E^{*,\mathrm{sc}} + E^{\mathrm{def,sc}} + E^{\mathrm{rot,sc}}. \quad (1)$$

After full acceleration (i.e., after relaxation of the deformation energy), the fission fragments are rotating and the total excitation energy is converted into intrinsic excitation energy E^* and collective rotational energy E^{rot},

$$\mathrm{TXE} = E_L^* + E_H^* + E_L^{\mathrm{rot}} + E_H^{\mathrm{rot}}, \quad (2)$$

where E_L^{rot}, E_H^{rot} are the rotational energies of the light and heavy fragments and E_L^*, E_H^* are their intrinsic excitation energies. The rotational energy of deformed fragments is due to angular-momentum-bearing collective modes, like bending or wriggling and as such is not drained from the intrinsic excitation energy available at scission [8].

Only the intrinsic excitation energy corresponding to $E_{L,H}^* = \mathrm{TXE} - E_{L,H}^{\mathrm{rot}}$ is treated within a Fermi-gas

approximation in aT^2, where a and T stand for the level-density parameter and the nuclear temperature. The partitioning between the two fragments is performed through a mass-dependent temperature ratio. This energy is dissipated by neutron emission until an excitation energy limit is reached. This limit is spin dependent through the neutron separation energy plus the rotational energy. When this limit is reached the neutron evaporation ends and the γ deexcitation can start (but is not yet implemented). Finally, as the kinematic relations are computed accounting for FF recoil and neutron emission, a simulation of the detection system can be undertaken.

A. Input experimental distributions

The primary probability density function is the experimental mass (A), nuclear charge (Z), and kinetic energy (KE) distribution $\mathcal{F}(A, \mathrm{KE}, Z)$. Here the parameters stand for the characteristics of the fragment before neutron emission.

1. *Mass A and kinetic energy* (KE)

We have used the experimental data from [9] where postneutron and preneutron emission masses are determined from the measurement of the FF kinetic energies using a double Frisch-grid ionization chamber. A NE213 neutron detector is used to measure in coincidence the prompt neutrons with the fission fragments. After basic mathematical arrangements the experimental $f(A, \mathrm{KE})$ matrix can be decomposed in a product of two normalized distribution functions:

$$f(A, \mathrm{KE}) = Y(A)\,\mathcal{N}(\langle \mathrm{KE}\rangle, \sigma_{\mathrm{KE}}), \tag{3}$$

where $Y(A)$ is the preneutron mass yield normalized to 2 and $\mathcal{N}(\langle \mathrm{KE}\rangle, \sigma_{\mathrm{KE}})$ is a mass-dependent Gaussian function characterized by a mean $\langle \mathrm{KE}\rangle$ and a standard deviation σ_{KE} (see Fig. 1). Due to too low statistics in the very asymmetric mass region and neglecting the ternary fission, we have considered a sample of 97 masses ranging from $A = 78$ to $A = 174$.

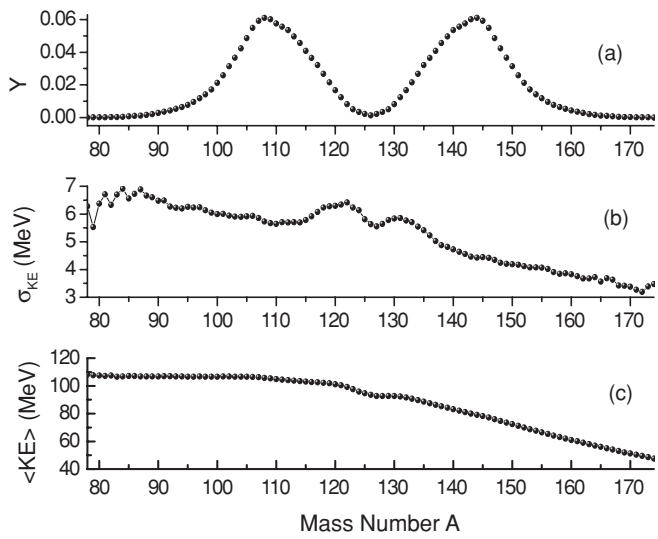

FIG. 1. ^{252}Cf experimental input data from [9]. Preneutron mass yield $Y(A)$ (a) and kinetic energy [distribution width σ_{KE} (b) and mean value $\langle \mathrm{KE}\rangle$ (c)].

2. *Nuclear charge Z*

In order to take into account the different isobars within a mass chain, we have considered a nuclear charge distribution $P(Z)$ which is almost Gaussian in shape [10] characterized by a mean Z_p value which corresponds to the most probable charge and a width parameter c,

$$P(Z) = \frac{1}{\sqrt{c\pi}} e^{-(Z-Z_p)^2/c}. \tag{4}$$

The width parameter c is related to a charge dispersion σ_Z through the Sheppard's correction [11],

$$c = 2\left(\sigma_Z^2 + 1/12\right). \tag{5}$$

Here we have considered a constant value for charge dispersion: $\langle \sigma_z \rangle = 0.59$ [12]. The most probable charges for light and heavy fragments (Z_p^L and Z_p^H, respectively) are obtained within the unchanged charge-density assumption (UCD) of the nuclear charge division. It means that the charge density Z/A of both the complementary fragments and the fissioning nucleus are conserved,

$$Z_{\mathrm{UCD}}^{L,H} = A_{L,H}\left(\frac{Z_f}{A_f}\right), \tag{6}$$

where f stands for the fissioning nucleus. It has been shown that the measured charges differ slightly from these most probable charges, the difference being the polarization function $\Delta Z(A)$ defined by

$$\Delta Z(A) = (Z_p - Z_{\mathrm{UCD}})_H = (Z_{\mathrm{UCD}} - Z_p)_L. \tag{7}$$

Most of the time a $-1/2$ mean value is considered even if an oscillating structure seems to be observed for various fissioning systems [12–15]. It has been argued, for instance, that for symmetrical fission, ΔZ tends to 0 and an abrupt change is observed near the $Z = 50$ closed proton shell. Recently some constrained Hartree-Fock-Bogoliubov calculations were performed by Younes and Gogny for thermal neutron-induced fission of ^{239}Pu in order to define scission configurations [16]. In the present work we have accounted for the slightly oscillating polarization function from Wahl [12] which was extended from $A = 170$ to $A = 174$.

Finally the complete distribution reads

$$\mathcal{F}(A, \mathrm{KE}, Z) = Y(A)\,\mathcal{N}(\langle \mathrm{KE}\rangle, \sigma_{\mathrm{KE}})P(Z). \tag{8}$$

It is then possible to sample a fission fragment (for instance, the light one) corresponding to a mass number A_L, a nuclear charge Z_L, and a kinetic energy KE_L. The complementary mass number A_H and charge Z_H of the heavy fragment are then deduced because of baryon number and charge conservation in binary fission. The kinetic energy KE_H of the heavy fission fragment is sampled as for the light one using a Box-Muler algorithm [17].

B. Excitation energy calculation

At this stage of the procedure we are able to calculate some basic quantities: the total kinetic energy of the fission fragments TKE and the energy release during the fission process Q based on binding energies from references [18] and [19]:

$$\mathrm{TKE} = \mathrm{KE}_L + \mathrm{KE}_H, \tag{9}$$

$$Q = B(A_L, Z_L) + B(A_H, Z_H) - B(A_f, Z_f). \tag{10}$$

The total number of ejectiles evaporated by the fission fragments is directly related to the excitation energy. For spontaneous fission, the total excitation energy (TXE) is simply related to the previous quantities

$$\mathrm{TXE} = Q - \mathrm{TKE}. \tag{11}$$

As the kinetic energy is sampled, the energy release in fission can be lower than the total kinetic energy, leading to a negative total excitation energy. These rare events are simply rejected by the code and represent less than 0.01% of the total number of fissions.

As mentioned before, one of the key points of the simulation is related to the partitioning of the excitation energy between the two fragments. Once fully accelerated, the intrinsic excitation energy of the rotating fission fragments is given by

$$E^* = \mathrm{TXE} - E_L^{\mathrm{rot}} - E_H^{\mathrm{rot}} = E_L^* + E_H^*, \tag{12}$$

where E_L^{rot}, E_H^{rot} are the rotational energies of the light and heavy fragments and E_L^*, E_H^* are their intrinsic excitation energies assumed to be used for neutron emission.

If we consider the nucleus as a Fermi gas the excitation energy can be related to the nuclear temperature T by

$$E^* = aT^2, \tag{13}$$

where a is the level-density parameter. The determination of the level-density parameter and the nuclear temperature are discussed in the two following subsections. The calculation of the rotational energy will be discussed in Sec. II D dealing with the excitation energy limit below which neutron emission is forbidden.

1. Level-density parameter

According to the Ignatyuk's model [20], in order to take into account the shell-effect damping for high excitation energies, this level-density parameter is energy dependent,

$$a = \overline{a}\left\{1 + \frac{\delta W}{U^*}(1 - e^{-\gamma U^*})\right\}. \tag{14}$$

In Eq. (14), $\overline{a}(A)$ is the asymptotic level-density parameter. δW accounts for the shell corrections that can be estimated by the difference between measured and calculated mass excesses (with a liquid-drop model, for example). $U^* = E^* - \Delta$ is an effective excitation energy function corrected by pairing Δ. Finally γ stands for the damping factor. Different sets of shell and pairing energy corrections are implemented: Gilbert-Cameron revisited and compiled for RIPL-1 [21], Myers-Swiatecky from RIPL-2 database [22], and Moller-Nix from RIPL-2 database [22]. Shell and pairing energy corrections are not defined in the same way by these various authors [23–25]. The entire set of parameters (a, δW, Δ, and γ) involved in Eq. (14) must be consistent so if shell and pairing corrections come from the Myers-Swiatecky set then the following pametrization is used for the asymptotic level-density parameter and damping factor:

$$\overline{a} = 0.0959A + 0.1468A^{2/3} \quad \text{and} \quad \gamma = 0.325A^{-1/3} \tag{15}$$

and for the Moller-Nix corrections

$$\overline{a} = 0.1125A + 1.22\ 10^{-4}A^2 \quad \text{and} \quad \gamma = 0.325A^{-1/3}. \tag{16}$$

In this work, the level-density parameters are calculated with the Myers and Swiatecki mass formula. In this case the shell corrections take into account the correction for the deformed nuclear shape based on β_2 and β_4 deformation parameters.

2. Nuclear temperature

A first assumption is to consider the same temperature for both fragments (as is done in [5] through the H1 hypothesis). Under this assumption both the fission fragments and the compound fissioning nucleus have the same temperature T related to the excitation energy within the Fermi-gas model by the following formula:

$$\frac{E_{\mathrm{int}}^*}{a} = \frac{E_L^*}{a_L} = \frac{E_H^*}{a_H}. \tag{17}$$

An iterative procedure is used to solve the "implicit" equation (E^* depends on the level-density parameter a which depends on the excitation energy E^*):

$$E_{L,H}^* = \frac{a_{L,H}}{a} E_{\mathrm{int}}^*. \tag{18}$$

We will see in Sec. III that this hypothesis is not able to reproduce the sawtooth shape of the prompt neutron multiplicity distribution $\overline{\nu}(A)$.

Consequently, a non-equitemperature model must be considered ($T_L = R_T T_H$) as originally proposed by Ohsawa [26]. The parameter R_T was chosen to be constant or linearly dependent of the mass number leading to the different phenomenological models which will be discussed in Sec. III.

C. Prompt neutron emission

Knowing the excitation energy of each fission fragment, the evaporation process (dissipation of energy) can start leading to the emission of neutrons and γ rays. In the center-of-mass frame, the energy ϵ of a neutron emitted by a nucleus at a given temperature T is sampled over a Weisskopf spectrum [27],

$$\phi(\epsilon) = \frac{\epsilon}{T^2} e^{-\epsilon/T}, \tag{19}$$

assuming that the cross section of the inverse process of compound nucleus formation is constant. The center-of-mass neutron energy ϵ is a random variate that can be easily sampled from this distribution since it is an Erlang distribution $Er(\alpha, \beta)$, which is a particular case of a γ distribution defined by

$$f_X(x) = \begin{cases} \frac{x^{\alpha-1}e^{-x/\beta}}{\beta^\alpha \Gamma(\alpha)} & \text{for } 0 \leqslant x < \infty \text{ and } \alpha > 0, \beta > 0 \\ 0 & \text{elsewhere,} \end{cases}$$

where $\Gamma(n+1) = n!$, $\alpha = 2$, and $\beta = T$. The algorithm consists of sampling and summing two (because $\alpha = 2$) independent exponential random variates as referred in [17]. The temperature T in Eq. (19) is the temperature of the residual nucleus after neutron emission and not the temperature of the compound nucleus before emission ([27,28]) so $T = T(A-1, Z, E^*)$,

$$T(A-1, Z, E^*) = \sqrt{\frac{E^*(A, Z) - S_n}{a(A-1, Z)}}, \tag{20}$$

where S_n is the neutron separation energy.

When a neutron is emitted with an energy ϵ in the center-of-mass frame, the excitation energy of the residual nucleus becomes

$$E^*(A-1, Z) = E^*(A, Z) - S_n - \epsilon. \tag{21}$$

After each neutron emission (isotropic in the center-of-mass frame), the transformation in the laboratory frame is performed using kinematic relations accounting for the FF recoil.

D. Excitation energy limit of the neutron evaporation process

The neutron evaporation ends when the excitation energy is lower than a given energy limit. In a first step we can simply consider the neutron separation energy S_n as a lower limit and then the residual excitation energy is available for deexcitation through γ rays. It will be shown in Sec. III that this crude approximation leads to an overestimation of the total average prompt neutron multiplicity $\overline{\nu}$ compared to experimental data. A higher energy limit is therefore required in order to reach a more consistent $\overline{\nu}$ value. We must consider that the fission fragment is a rotating nuclei and consequently we add a rotational energy in addition of the neutron separation energy of the ground state,

$$E^*_{\text{lim}} = S_n + E^{\text{rot}}. \tag{22}$$

The collective rotational energy is approximated by the rotating liquid-drop model. In such a macroscopic model, the rotational energy of a fission fragment is given by

$$E^{\text{rot}} = \frac{\hbar^2 J(J+1)}{2\mathcal{J}}, \tag{23}$$

where J stands for the total angular momentum and $\mathcal{J}$ stands for the moment of inertia. These excited states have a minimum energy for a given angular momentum and correspond to the so-called yrast line under which no state is available. This formulation of the rotational energy is used in Eq. (12) for the partitioning of the excitation energy after full acceleration. In a quantum-mechanical description, spherical fission fragments cannot exhibit collective rotation and Eq. (23) is no longer valid. This has a negligible impact on the results that will be presented in Sec. III because spherical FF have a low initial excitation energy and they cannot emit as many neutrons (configuration near magic shells) no matter what the considered excitation energy limit is [S_n or $S_n(J)$]. Under these simple assumptions the neutron evaporation occurs when the excitation energy is higher than the neutron separation energy above the yrast line:

$$E^* > S_n(J) \quad \text{where} \quad S_n(J) = S_n + E^{\text{rot}}(J). \tag{24}$$

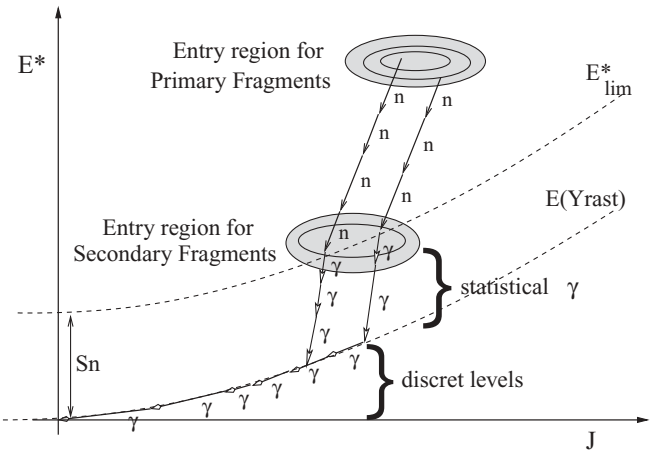

FIG. 2. Schematic representation of the evaporation of the fission fragments in the (E^*, J) plan. Primary fragments dissipate excitation energy E^* through neutron emission until $E^* < S_n + E^{\text{rot}}$ while secondary fragments dissipate energy through γ rays.

When the condition given by Eq. (24) is no longer satisfied, γ deexcitation can start. First, statistical transitions of low multipolarities ($E1$ and $M1$) carry away a large amount of excitation energy and second, discrete γ rays from yrast bands occur. The γ deexcitation is not yet implemented and will be studied in future developments; nevertheless, the remaining excitation energy needed for γ emission is obviously available. Figure 2 shows a typical deexcitation process in a (E^*, J) plan. Primary fragments stop emitting neutrons when the final state (E^*, J) is lower than $E^*_{\text{lim}} = S_n(J)$. These secondary fragments dissipate the remaining excitation energy and angular momentum by γ-ray transitions.

Accounting for E^{rot} in this excitation energy limit favors the γ deexcitation at high spin and therefore allows us to simulate the n/γ competition as already suggested by Grover and Gilat [29].

1. Fission fragment angular momentum

The primary fission fragment angular momentum involved in Eq. (23) is sampled from a probability of states from [30]:

$$P(J) \propto (2J+1)\, e^{-(J+1/2)^2/B^2}, \tag{25}$$

where B is almost equal to the root mean square value of $J + \frac{1}{2}$. The best agreement with experimental data (see Sec. III) is achieved by considering as input data: $B = 6\hbar$

for light fission fragments and $B = 7.2\hbar$ for heavy fragments. Even if these average values have to be replaced by a more rigorous treatment[1] in a future release of the code, they are consistent with the Wilhelmy's observations based on 21 even-even deformed fragments [31]. In Wilhelmy's paper, the ^{252}Cf FF average angular momentum is around $(7 \pm 2)\hbar$ and the heavy fission fragments have around 20% greater angular momentum than the light ones.

2. *Moment of inertia* $\mathcal{J}$

For the determination of the nuclear moment of inertia $\mathcal{J}$ involved in Eq. (23), we have considered two extreme cases: a deformed rigid body and an irrotational flow obeying hydrodynamical equations as described in Ref. [32]. The rigid body moment of inertia is given by

$$\mathcal{J}_{\text{rigid}} = \tfrac{2}{5} A M R^2 (1 + 0.31\beta + 0.44\beta^2 + \cdots), \qquad (26)$$

where A, M, R, and β, respectively, stand for the mass number, the nucleon mass, the radius ($R = 1.2A^{1/3}$ fm), and the quadrupole deformation parameter of the nucleus in its ground state taken from Ref. [22]. The moment of inertia of the fluid irrotational model is given by

$$\mathcal{J}_{\text{irrot}} = \tfrac{2}{5} A M (\Delta R)^2, \qquad (27)$$

where $\Delta R = R_3 - R_\perp$ stands for the difference between major and minor semiaxes which can be related to the deformation parameter through

$$\Delta R = R_3 - R_\perp = \frac{3}{4}\sqrt{\frac{5}{\pi}} R\beta. \qquad (28)$$

By replacing (28) in (27) we find the other expression used in [33] or [34],[2]

$$\mathcal{J}_{\text{irrot}} = \frac{9}{8\pi} A M R^2 \beta^2. \qquad (29)$$

Nevertheless it is well established that a nucleus is neither a rigid body nor a fluid inside a rotating ellipsoidal vessel: $\mathcal{J}_{\text{irrot}} < \mathcal{J} < \mathcal{J}_{\text{rig}}$. For instance, considering the ^{164}Er first excited state 2^+ at 91.4 keV, from a numerical application of Eq. (23) a value of $\hbar^2/2\mathcal{J} = 15$ keV is deduced using $\beta \simeq 0.3$. The rigid body model gives $\hbar^2/2\mathcal{J}_{\text{rig.}} = 6$ keV while the fluid model gives $\hbar^2/2\mathcal{J}_{\text{irrot}} = 90$ keV. Consequently we must then consider an intermediate moment of inertia value lying between these two extreme configurations.

III. RESULTS AND DISCUSSION

Among other distributions that can be achieved by the code, the most important are listed here:

(i) $\overline{\nu}(A, \text{TKE})$, $\overline{\nu}(A)$, and $\overline{\nu}(\text{TKE})$, the average prompt neutron multiplicity as a function of the total kinetic energy and/or mass fragment.
(ii) $\langle\epsilon\rangle(A)$ and $\langle E\rangle(A)$, the mean neutron energies in the center of mass and laboratory frames for each mass.
(iii) $\phi(\epsilon, A)$ and $N(E, A)$, the neutron spectrum in the center of mass and laboratory frames for each mass.
(iv) $\phi(\epsilon)$ and $N(E)$, the average neutron spectra in the center of mass and laboratory frames.
(v) $P(\nu)$, the prompt neutron multiplicity distribution.
(vi) $\langle E_\gamma\rangle(A)$, the mean energy deposited by prompt γ-rays for each mass.
(vii) Etc.

The experimental data used for comparison in this section are the following:

(i) Budtz-Jørgensen and Knitter [35] for $\overline{\nu}(A)$, $\overline{\nu}(\text{TKE})$ and $\langle\epsilon\rangle(A)$.
(ii) Hambsch *et al.* [36] for $\overline{\nu}(A)$ (preliminary results).
(iii) Bowman *et al.* [37] for $\overline{\nu}(A)$ and $\overline{\nu}(\text{TKE})$.
(iv) Nifenecker *et al.* [38] for $\overline{\nu}(\text{TKE})$ and $\langle E_\gamma\rangle(A)$.
(v) Vorobyev [39] for $\overline{\nu}$ and $P(\nu)$.
(vi) Boldeman [40] for $\overline{\nu}$ and $P(\nu)$.
(vii) Santi and Miller [41] for $P(\nu)$.

Various models are proposed and analyzed. As the number of neutrons evaporated by a fragment is directly related to the nuclear temperature and the excitation energy, these models differ by the temperature ratio between the two complementary fragments after full acceleration ($R_T = T_L/T_H$), the excitation energy limit for neutron emission (E^*_{limit}), and the moment of inertia $\mathcal{J}$ involved in the rotational energy if needed.

A. Influence of a constant temperature ratio with $E^*_{\text{lim}} = S_n$

In this case $E^{\text{rot}} = 0$ in Eq. (12) and Eq. (22) and the neutron separation energy S_n is considered as an upper limit below which the neutron evaporation is forbidden. Furthermore, if we consider an equipartition of the temperature between the two fragments ($R_T = 1$) then the distribution of the multiplicity as a function of the mass number does not show the well known sawtooth shape (see Fig. 3). Similar results were already reported in the Lemaire's paper [5] obtained with the H1 hypothesis. The $\overline{\nu}_L/\overline{\nu}_H$ ratio is inverted as mentioned by Talou [42] and $\overline{\nu}$ is strongly overestimated (see Table I).

If we consider that the temperature of the light fragment is 25% higher than the heavy one, a sawtooth can be observed with $\overline{\nu}_L > \overline{\nu}_H$ (see Fig. 3 and Table I). The temperature ratio plays a role in the partition of the multiplicity between light and heavy fragments but not necessarily in the total average value: $\overline{\nu}$ is almost unchanged (10% higher than the measurement) but the $\overline{\nu}_L/\overline{\nu}_H$ ratio is different.

B. Influence of the moment of inertia involved in $E^*_{\text{lim}} = S_n + E^{\text{rot}}$ with $R_T = 1.25$

We now consider $S_n + E^{\text{rot}}$ as an excitation energy limit for the neutron evaporation with again $R_T = T_L/T_H = 1.25$.

[1] For instance, it is well stated that B is related to the moment of inertia and the nuclear temperature: $B = 2\mathcal{J}T/\hbar^2$.

[2] Note that the square power is missing in Eq. (5.19) from Ref. [34] involving β instead of β^2.

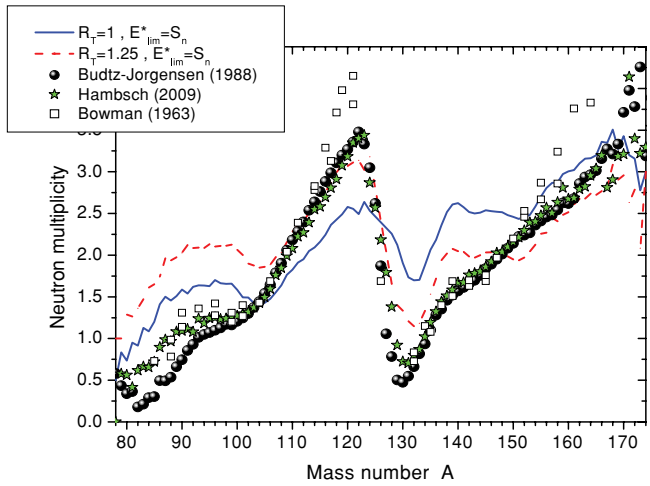

FIG. 3. (Color online) Average prompt neutron multiplicity as a function of mass calculated with $R_T = 1$ and $E^*_{\rm lim} = S_n$ compared with measurements from Budtz-Jørgensen and Knitter [35], Hambsch *et al.* [36], and Bowman *et al.* [37].

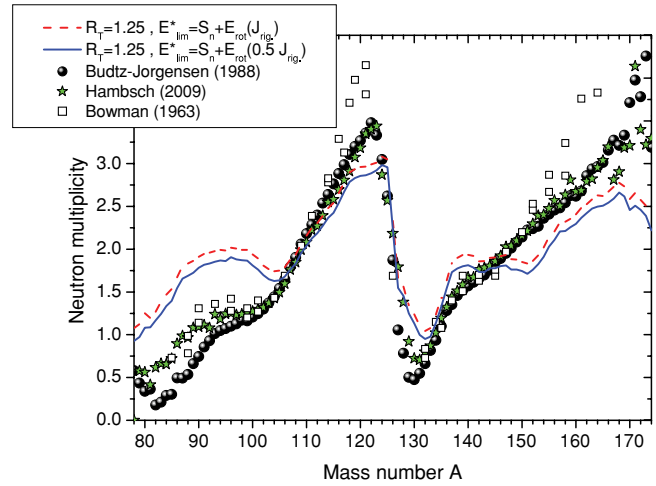

FIG. 4. (Color online) Same as Fig. 3 with $R_T = 1.25$ and $E^*_{\rm lim} = S_n + E^{\rm rot}$ involving two sets of moment of inertia ($\mathcal{J} = \mathcal{J}_{\rm rig.}$ and $\mathcal{J} = 0.5\mathcal{J}_{\rm rig.}$).

If the moment of inertia involved in the rotational energy $E^{\rm rot}$ is a rigid body moment of inertia [$\mathcal{J}_{\rm rig.}$ given by Eq. (26)], the $\overline{\nu}_L$, $\overline{\nu}_H$, and $\overline{\nu}$ values are a bit more improved (see Table I) but the sawtooth is not entirely satisfactory (see Fig. 4).

With an irrotational model for the moment of inertia [$\mathcal{J}_{\rm irrot.}$ given by Eq. (27)], results become completely wrong because the moment of inertia is directly related to the square of the deformation parameter and appears in the denominator for the rotational energy calculation [Eq. (23)]. Therefore, a fission fragment with a small deformation will have a low excitation energy for neutron emission [Eq. (12)], leading to a drastic underestimation of $\overline{\nu}(A)$.

With an intermediate moment of inertia (50% of a rigid body moment) the overall distribution is not yet satisfactory (see Fig. 4) even if the total average multiplicities $\overline{\nu}_L$, $\overline{\nu}_H$, and $\overline{\nu}$ are consistent with the experimental data (see Table I). With a constant temperature ratio, it is definitively not possible to reproduce the sawtooth shape of the average prompt neutron multiplicity as a function of mass.

Table I summarizes the influence of a constant temperature ratio and a spin-dependent excitation energy limit on the total average prompt neutron multiplicity.

TABLE I. Total average prompt neutron multiplicities for various models.

R_T	$E^*_{\rm limit}$	$\mathcal{J}$	$\overline{\nu}_L$	$\overline{\nu}_H$	$\overline{\nu}$
1.	S_n		1.82	2.44	4.26
1.25	S_n		2.28	1.93	4.21
1.25	$S_n + E^{\rm rot}$	$\mathcal{J}_{\rm rig.}$	2.18	1.83	4.01
1.25	$S_n + E^{\rm rot}$	$0.5\mathcal{J}_{\rm rig.}$	2.07	1.71	3.78
Vorobyev *et al.* [39]			2.051	1.698	3.756(31)
Boldeman [40]					3.757

C. Mass-dependent temperature ratio and spin-dependent excitation energy limit

As shown in the preceding section, a constant temperature ratio cannot reproduce properly the experimental sawtooth. Here we will consider a mass-dependent temperature ratio which is defined by the following physical constraints based on nucleus deformation at scission. We consider three typical fragment configurations for which the ratio R_T should be lower, equal,or greater than 1:

(i) For symmetric fission we expect the same temperature for both complementary fragments and then $R_T = 1$.

(ii) For light mass number $A_L = 120$, R_T is maximum because in the case of ^{252}Cf the complementary heavy fragment is nearly spherical with 132 nucleons (corresponding to $Z = 50$ closed proton shell and $N = 82$ closed neutron shell). Consequently the light fragment $A_L = 120$ gains the major part of the total excitation energy associated with a higher temperature compared to its double magic complementary partner.

(iii) For very asymmetric fission the heavy fragment is more deformed than the light fragment because the latter becomes shell stabilized. The light fragment can be nearly spherical with a $Z = 28$ closed proton shell and an $N = 50$ closed neutron shell, leading to a temperature lower than the temperature of the heavy fragment ($R_T < 1$). This fact has been already mentioned by Denschlag [43]. Therefore, as it has been argued by Gönnenwein [44], the ratio of temperatures should be reversed ($R_T < 1$).

A simple composition of two linear laws is assumed between these three key configurations as shown in Fig. 5. In addition, the excitation energy limit is spin dependent, involving a moment of inertia equal to 50% of the rigid body moment of inertia.

With this refined model, we will now discuss the average prompt neutron multiplicity, the distribution of the prompt neutron multiplicity, the prompt fission neutron energy, the

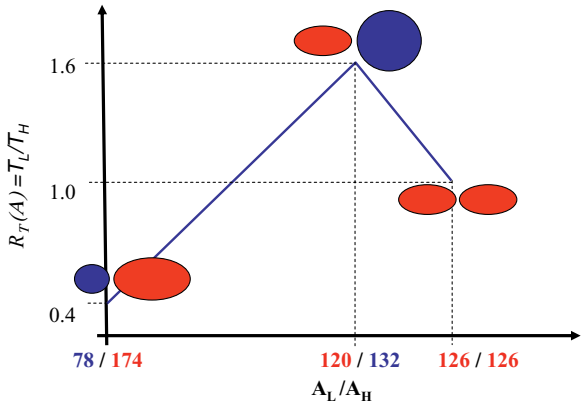

FIG. 5. (Color online) Macroscopic constraints for the determination of the temperature ratio law $R_T(A)$. For mass split 78/174 the light FF is near spherical and then its temperature is lower than its heavy partner, leading to a minimum $R_T < 1$. For mass split 120/132 the situation is reversed and the heavy FF is near spherical with a higher temperature than its light partner, leading to a maximum $R_T > 1$. Finally for symmetric mass split 126/126 the temperature is the same and then $R_T = 1$.

available energy for γ emission, and lastly, the total prompt energy release.

1. *Average prompt neutron multiplicity as a function of mass* $\overline{\nu}(A)$

The sawtooth description is clearly improved as observed in Fig. 6 as well as the total average values (see Table II). It would be possible to better reproduce the sawtooth by adjusting the temperature ratio law for each mass but this is not the actual goal of the code. Other fission observables are not sufficiently known and mass resolution from experimental data is not precise enough to make a confident adjustment.

2. *Average prompt neutron multiplicity as a function of total kinetic energy* $\overline{\nu}$(TKE)

The average prompt fission neutron multiplicity is plotted as a function of the fission fragment total kinetic energy

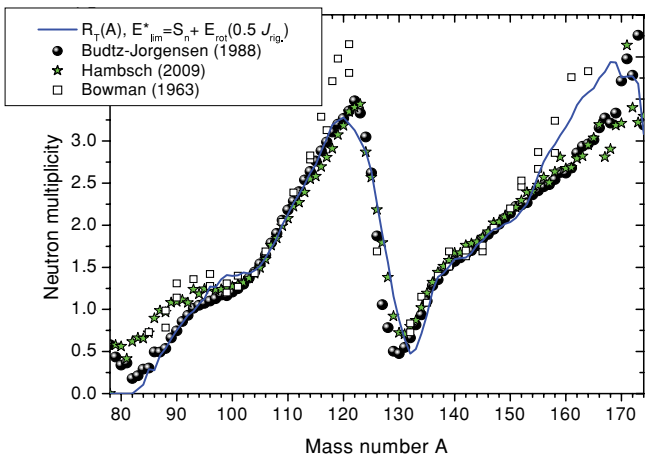

FIG. 6. (Color online) Same as Fig. 3 with the refined model.

TABLE II. Total average prompt neutron multiplicities calculated with the refined model and compared with experimental data.

R_T	E^*_{limit}	$\mathcal{J}$	$\overline{\nu}_L$	$\overline{\nu}_H$	$\overline{\nu}$
$R_T(A)$	$S_n + E^{\text{rot}}$	$0.5\mathcal{J}_{\text{rig.}}$	2.06	1.70	3.76
Vorobyev *et al.* [39]			2.051	1.698	3.756(31)
Boldeman [40]					3.757

TKE in Fig. 7. Our Monte Carlo simulation does not fit the data from Bowman [37] but is in good agreement with the Budtz-Jørgensen data [35], except in the high total kinetic energy region: above 190 MeV, our calculation underestimates the prompt neutron number. A similar trend was reported by Kornilov in Ref. [45] and explained by the possible existence of scission neutrons which are not taken into account here.

In addition, we have to keep in mind that, in the present work, neutrons are evaporated following a Weisskopf spectrum which requires among others that the neutron energy in the center of mass has to be small compared to the residual FF excitation energy [27]. This requirement could be not satisfied when the kinetic energy is too high, yielding to a wrong estimation of the neutron multiplicity.

The inverse slope of a straight line fit of the average multiplicity as a function of TKE, given by $-(\delta\overline{\nu}/\delta\text{TKE})^{-1}$, is about 13 MeV/$n$, which is in quite good agreement with published experimental data like those of Budtz-Jørgensen *et al.* [35] and Nifenecker *et al.* [38] (see Table III). As reported by Nifenecker this is not the energy necessary to emit one more neutron, especially because different mass and kinetic energies are involved.

We want to emphasize that calculation shows two different slopes in $\overline{\nu}$(TKE) below and above around 180 MeV. This nonlinear behavior can be understood by looking at Fig. 8 where the contributions of both light and heavy FF

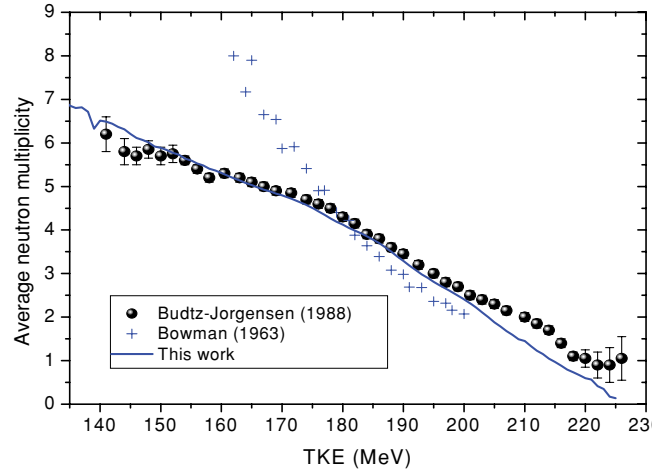

FIG. 7. (Color online) Average prompt neutron multiplicity as a function of the fission fragment total kinetic energy compared with Budtz-Jørgensen *et al.* [35]. Data from Bowman *et al.* [37] are also reported.

TABLE III. Inverse slope of the average prompt neutron multiplicity as a function of the fission fragment total kinetic energy TKE.

Authors	$-(\delta\overline{\nu}/\delta\mathrm{TKE})^{-1}$ (MeV/n)
Nifenecker *et al.* [38]	13.0
Budtz-Jørgensen *et al.* [35]	12.5
This work	13.0

are plotted. Only the heavy FF has a rather linear behavior while the light one exhibits two different trends: an increase (decrease) of the neutron number below (above) around 180 MeV. Additionally, the heavy fission fragment is not able to emit neutrons when the total kinetic energy is higher than 210 MeV while at very low TKE (<135 MeV) it is the main neutron emitter. Figure 9 depicts these observations in a two-dimensional plot.

3. *Distribution of the prompt neutron multiplicity $P(\nu)$*

Another important parameter related to prompt fission neutrons is the prompt neutron multiplicity distribution. As data of Vorobyev [39], Boldeman [40], and Santi [41] are very close, our results are compared only with data of Ref. [39] for reasons of clarity in Fig. 10.

Both light and heavy fragment contributions are also given, showing a nice agreement with experimental data. Obviously the prompt neutron multiplicity distribution $P(\nu)$ is mainly governed by, at least, the following parameters:

(i) The excitation energy limit for the neutron evaporation process.
(ii) The competition between neutrons and gammas.
(iii) The angular momentum carried away by neutrons (here $\Delta J = 1\hbar$ is assumed).

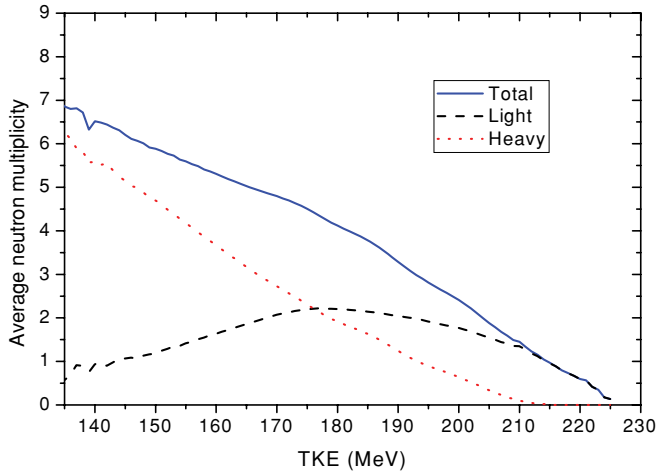

FIG. 8. (Color online) Average prompt neutron multiplicity as a function of the fission fragment total kinetic energy TKE for the light, the heavy, and the pair of fragments.

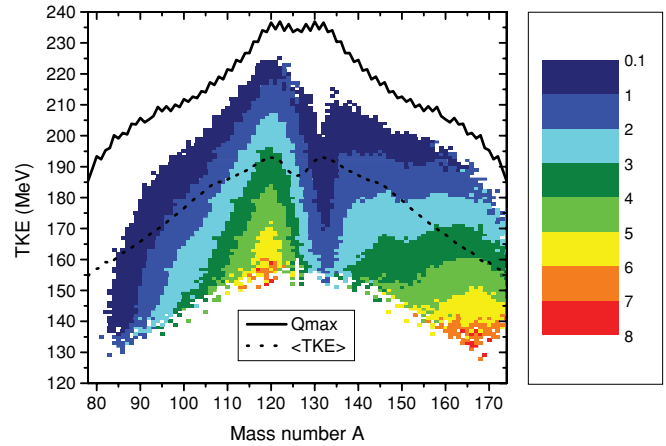

FIG. 9. (Color) Average prompt neutron multiplicity as a function of mass number A and total kinetic energy TKE [$\overline{\nu}(A, \mathrm{TKE})$]. Q_{max} and $\langle\mathrm{TKE}\rangle$ are also represented to guide the eyes.

4. *Average prompt fission neutron energy $\langle\epsilon\rangle(A)$*

The average neutron energy in the center of mass as a function of FF mass $\langle\epsilon\rangle(A)$ is shown in Fig. 11 and compared with data from Ref. [35].

A good agreement is achieved except in the $A = 125 - 140$ mass region. This discrepancy was already observed by Lemaire [5] and Kornilov [45]. The Kornilov's calculations are based on the level-density systematic of Ignatyuk but corrected by a factor lying between 0.4 and 1.25 applied on the heavy FF excitation energy calculated under a $R_T = 1$ assumption.

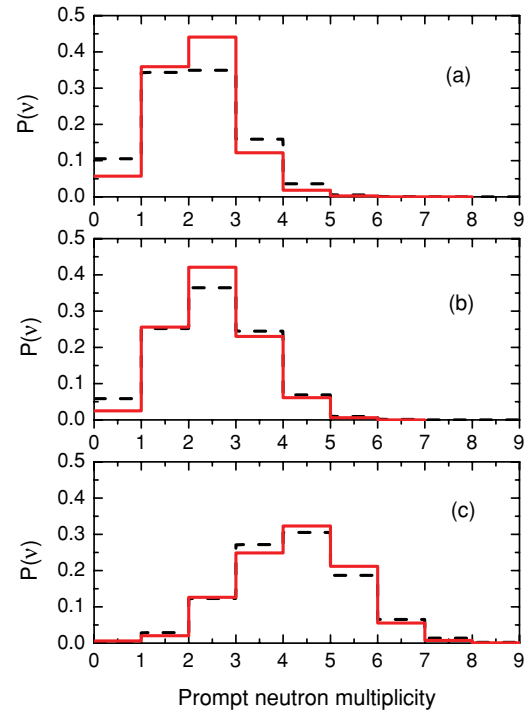

FIG. 10. (Color online) Prompt neutron multiplicity distributions for heavy (a), light (b), and both (c) fission fragments. The dashed line correponds to experimental data from Vorobyev [39]. The full line is the result obtained with our refined model.

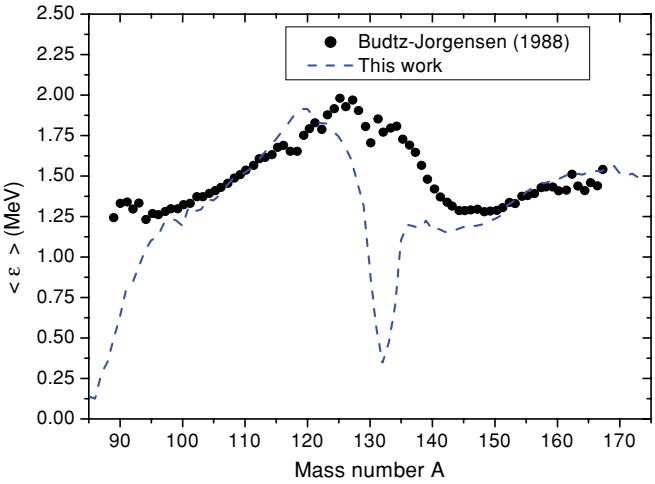

FIG. 11. (Color online) Average center-of-mass neutron energy as a function of mass number compared with experimental data from [35].

In this way the author can fit the experimental sawtooth but cannot reproduce the $\langle\epsilon\rangle(A)$ behavior. As mentioned by Kornilov, if the Fermi-gas model is valid, a positive correlation is expected between the multiplicity and the energy of the emitted neutrons. It is confirmed by our calculation (see Figs. 6 and 11) but in conflict with experimental data. For instance, when $\overline{\nu} \leqslant 1.25$ ($A \leqslant 95$ and $A \in [125, 140]$) a strong underestimation of $\langle\epsilon\rangle$ with respect to experimental data is found, meaning that the Fermi-gas model cannot be applied anymore in these mass regions, e.g., for fission fragments with low excitation energy.

In addition, as already said previously, the Weisskopf's statistics theory used here for neutron emission is valid only when the remaining intrinsic excitation energy is still high after neutron emission: this could be no longer the case for high (low) kinetic (excitation) energies.

Note that Gilbert and Cameron [23] proposed in their so-called composite level-density formula to use a constant temperature model (CTM) for low excitation energies and a Fermi-gas model for high excitation energies. Moreover, very recently Schmidt and Jurado [46] are claiming that the CTM has to be used for level-density calculations up to 20 MeV.

5. *Prompt fission neutron spectra $N(E)$*

Since ^{252}Cf neutron spectrum is an international reference standard for metrological applications, important efforts have been done to produce a revised evaluation [47]. In Fig. 12 a comparison between the neutron spectrum in the laboratory frame calculated with our model and both Maxwellian ($T_M = 1.42$) and Manhart's evaluation is shown.

In our simulation the neutron spectrum is slightly underestimated below 500 keV and slightly overestimated above 10 MeV. Figure 13 shows the ratio of the calculated prompt neutron spectrum to the Manhart's evaluation and the agreement is encouraging with a discrepancy lower than 5% from 250 keV to 8 MeV. Nevertheless, this could be improved by taking into account an energy-dependent cross section for the inverse process of the compound nucleus formation as already reported by Madland and Nix in Ref. [1]. Another way of improvement could be to account for the anisotropy of neutron emission as proposed by Terrell [48] and recently applied by Hambsch in Ref. [49].

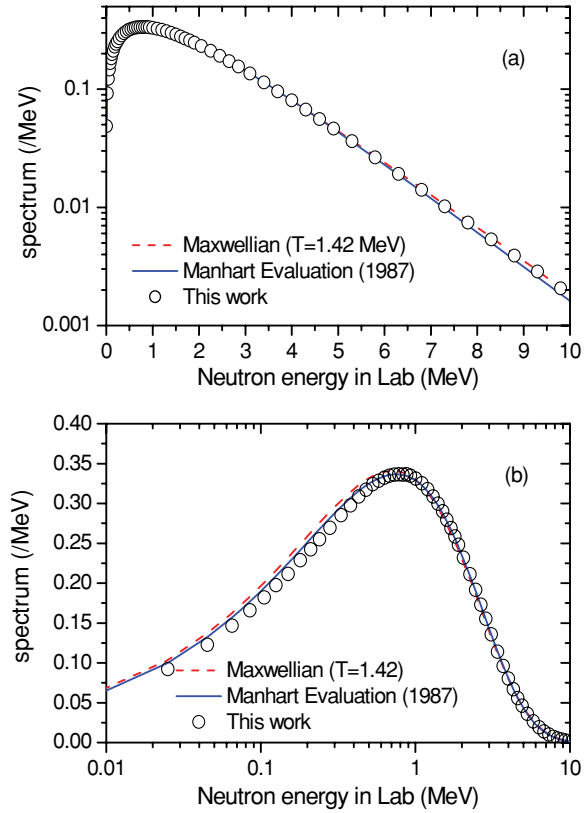

FIG. 12. (Color online) Neutron spectrum compared with a Maxwellian ($T_M = 1.42$) and the Manhart evaluation. The spectrum is lying between the Maxwellian and the Manhart's evaluation above few MeV (a) and is slightly underestimated at low energies (b).

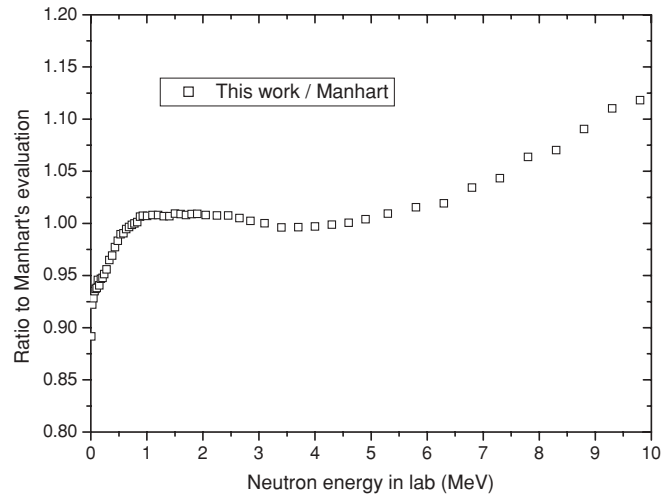

FIG. 13. Ratio of the calculated neutron spectrum to the Manhart's evaluation.

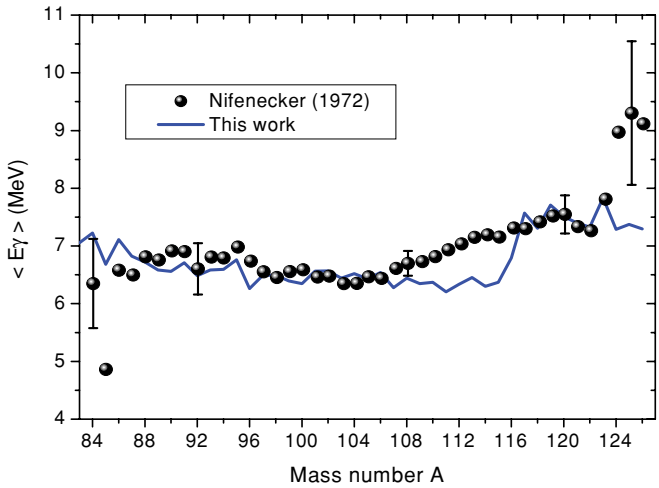

FIG. 14. (Color online) Total excitation energy available for γ deexcitation $\langle E_\gamma \rangle$ as a function of the light fragment mass number, compared with Nifenecker's data [50].

6. Available energy for prompt γ emission

Even if the γ-rays deexcitation is not yet implemented, the average fission fragment excitation energy leading to prompt γ emission $\langle E_\gamma \rangle$ is available for each secondary fragment. This quantity is summed for each FF pair and represented as a function of the light FF mass in Fig. 14. An overall good agreement can be observed except in the symmetric region where the calculation seems to underestimate experimental data from Ref. [50]. In addition the total average value weighted by the mass yields $\langle E_\gamma \rangle = 6.77$ MeV, which is in perfect agreement with the Nifenecker value (6.82 MeV) and other experimental data (see Table IV).

7. Total prompt energy release

The average total kinetic energy before neutron emission $\langle \mathrm{TKE} \rangle$ and after neutron emission $\langle \mathrm{TKE} \rangle^{\mathrm{post}}$, the prompt fission γ-ray energy $\langle E_\gamma \rangle = \overline{M}_\gamma \langle \epsilon_\gamma \rangle$ and the average energy deposited by prompt neutrons $\langle E_n \rangle = \overline{\nu} \langle E \rangle$ can be estimated with a good agreement. Table IV gives a comparison with experimental data of energy released by neutrons, gammas, and fission fragments during fission.

The average postneutron emission total FF kinetic energy $\langle \mathrm{TKE} \rangle^{\mathrm{post}}$ is very consistent with the recommended value by Gönnenwein [181.35 ± 1.3 MeV for ^{252}Cf(sf) [51]], meaning that both the initial experimental distributions and the whole evaporation process are satisfactory. The reference value for the mean energy deposited by neutrons is given by $\langle E_n \rangle = \overline{\nu} \langle E \rangle = 8.00$ MeV where $\overline{\nu} = 3.756$ is taken from Ref. [39] and $\langle E \rangle = 2.13$ MeV comes from the Manhart's neutron spectrum in the laboratory frame taken from Ref. [47]. Our calculation gives $\overline{\nu} = 3.76$ and $\langle E \rangle = 2.14$ MeV, leading to $\langle E_n \rangle = 8.04$ MeV in perfect agreement with the reference data. Finally, as mentioned in the previous section, the total average prompt γ energy is also in good agreement with experimental data.

TABLE IV. Mean energy release in fission by FF, prompt neutrons, and gammas, compared with experimental data.

Mean energy release (prompt component)	This work (MeV)	Experiment (MeV)
$\langle \mathrm{TKE} \rangle$	184.46	184.1 [51]
$\langle \mathrm{TKE} \rangle^{\mathrm{post}}$	181.64	181.35 [51]
$\langle E_n \rangle$	8.04	8.00 (3.756 [39] × 2.13 [47])
$\langle E_\gamma \rangle$	6.77	6.82 [50]
		7.08 [52]
		6.84 ± 0.3 [53]
		6.7 ± 0.4 [54]

IV. CONCLUSION

Various phenomenological models have been implemented in a Monte Carlo code simulating the fission fragment evaporation process. These models were tested against experimental data for spontaneous fission of ^{252}Cf. The most important parameters involved in the various models are the repartition of the excitation energy between the complementary fragments, the excitation energy limit for neutron emission which involves the fission fragment moment of inertia $\mathcal{J}$, and their initial spin distribution. This work highlights that our refined model is suitable to reproduce with an overall good agreement the major distributions related to prompt fission neutrons as well as the prompt component of the energy release in fission. In this model the key parameters are the mass-dependent temperature ratio law which governs the excitation energy partition between the two primary fragments, the excitation energy limit for neutron emission, which is given by a spin-dependent neutron separation energy $S_n(J) = S_n + E^{\mathrm{rot}}$, and lastly, a moment of inertia equal to 50% of a rigid spheroid moment of inertia ($\mathcal{J} = 0.5\mathcal{J}_{\mathrm{rig.}}$).

Models and assumptions discussed in this paper could be upgraded in different ways:

(i) Nuclear charge division in addition of unchanged charge density (UCD): equal charge displacement (ECD), minimum potential energy (MPE), etc.
(ii) Initial partitioning of the intrinsic, deformation, and collective energies between both fragments at scission.
(iii) Rotational energy and realistic moment of inertia involved in the excitation energy limit for neutron evaporation.
(iv) Initial fission fragment spin distribution needed for a reliable description of the neutron/γ competition.
(v) Possible additional neutron source (scission neutrons).

Additionally, an output file is generated during the Monte Carlo run, storing the nuclear characteristics of the fission fragments (mass number, kinetic energy, excitation energy at each evaporation stage, energy of evaporated neutrons, etc.) for each fragment history. A root tree [55] is then generated in order to user-friendly analyze the whole data inside the root data analysis framework. This specific tool is still under construction and will allow us to analyze any kind of distribution in any dimension with or without constraints and some very particular events, such as cold fission, neutron multiplicity for very low and very high kinetic energy, and so on.

[1] D. G. Madland and J. R. Nix, Nucl. Sci. Eng. **81**, 213 (1982).
[2] D. G. Madland, in Report No. INDC(NDS)-220, 1989, p. 259.
[3] G. Vladuca and A. Tudora, Ann. Nucl. Energy **28**, 1643 (2001).
[4] A. Tudora, Ann. Nucl. Energy **33**, 1030 (2006).
[5] S. Lemaire, P. Talou, T. Kawano, M. B. Chadwick, and D. G. Madland, Phys. Rev. C **72**, 024601 (2005).
[6] J. Randrup and R. Vogt, Phys. Rev. C **80**, 024601 (2009).
[7] R. Vogt, J. Randrup, J. Pruet, and W. Younes, Phys. Rev. C **80**, 044611 (2009).
[8] F. Gönnenwein *et al.*, in *Proceedings of Seminar on Fission, Corsendonk Priory, Belgium, 2007*, edited by C. Wagemans *et al.* (World Scientific, Singapore, 2008), p. 3.
[9] N. Varapai, F.-J. Hambsch, S. Oberstedt, O. Serot, G. Barreau, N. Kornilov, S. Zeinalov, in *Proceedings of the International Workshop on Nuclear Fission and Fission Product Spectroscopy, Cadarache, France, 2005*, edited by H. Goutte *et al.*, AIP Conf. Proc. No. 798 (AIP, New York, 2005), p. 369.
[10] A. C. Wahl, R. L. Ferguson, D. R. Nethaway, D. E. Troutner, K. Wolfsberg, Phys. Rev. C **126**, 1112 (1962).
[11] R. Vandenbosch and J. R. Huizenga, *Nuclear Fission* (Academic, New York, 1973).
[12] A. C. Wahl, At. Data Nucl. Data Tables **39**, 1 (1988).
[13] J. P. Bocquet and R. Brissot, Nucl. Phys. A **502**, 213c (1989).
[14] H. Naik, S. P. Dange, R. J. Singh, and S. B. Manohar, Nucl. Phys. A **612**, 143 (1997).
[15] H. Naik, R. J. Singh, and R. H. Iyer, J. Phys. G **30**, 107 (2004).
[16] W. Younes and D. Gogny, in *Proceedings of the 4th International Workshop on Nuclear Fission and Fission Product Spectroscopy, Cadarache, France, 2009*, edited by A. Chatillon *et al.*, AIP Conf. Proc. No. 1175 (AIP, New York, 2010), p. 3.
[17] R. Y. Rubinstein, *Simulation and the Monte Carlo Method* (Wiley, New York, 1981).
[18] A. H. Wapstra, G. Audi, and C. Thibault, Nucl. Phys. A **729**, 129 (2003).
[19] G. Audi, A. H. Wapstra, and C. Thibault, Nucl. Phys. A **729**, 337 (2003).
[20] A. V. Ignatyuk, G. N. Smirenkin, and A. S. Tishin, Sov. J. Nucl. Phys. **21**, 255 (1975).
[21] *Reference Input Parameter Library*, IAEA Report No. IAEA-TECDOC-1034, 1998.
[22] *Reference Input Parameter Library-2*, IAEA Report No. IAEA-TECDOC-1506, 2006.
[23] A. Gilbert and A. G. W. Cameron, Can. J. Phys. **43**, 1446 (1965).
[24] W. D. Myers and W. J. Swiatecki, Nucl. Phys. A **601**, 141 (1996).
[25] P. Moller, J. R. Nix, W. D. Myers, and W. J. Swiatecki, At. Data Nucl. Data Tables **59**, 185 (1995).
[26] T. Ohsawa, in IAEA Report No. INDC(NDS)-251, 1991, p. 71.
[27] V. F. Weisskopf, Phys. Rev. **52**, 295 (1937).
[28] J. M. Blatt and V. F. Weisskopf, *Theoretical Nuclear Physics* (Springer-Verlag, New York, 1979).
[29] J. R. Grover and J. Gilat, Phys. Rev. **157**, 802 (1967).
[30] D. De Frenne, in *The Nuclear Fission Process*, edited by C. Wagemans (CRC Press, Boca Raton, 1991), p. 475.
[31] J. B. Wilhelmy, E. Cheifetz, R. C. Jared, S. G. Thompson, H. R. Bowman, and J. O. Rasmussen, Phys. Rev. C **5**, 2041 (1972).
[32] A. Bohr and B. Mottelson, Dan. Mat. Fys. Medd. **30**, 1 (1955).
[33] D. R. Inglis, Phys. Rev. **96**, 1059 (1954).
[34] K. S. Krane, *Introductory Nuclear Physics* (Wiley, New York, 1988).
[35] C. Budtz-Jørgensen and H. H. Knitter, Nucl. Phys. A **490**, 307 (1988).
[36] F.-J. Hambsch, S. Oberstedt, S. Zeynalov, N. Kornilov, I. Fabry, R. Borcea, and A. Al-Adili, in *Proceedings of the International Workshop on Compound Nuclear Reactions and Related Topics*, Bordeaux, France, 2009, edited by L. Bonneau *et al.* (EDP Sciences, Les Ulis, France, 2009), p. 07002.
[37] H. R. Bowman, J. C. D. Milton, S. G. Thompson, and W. J. Swiatecki, Phys. Rev. **129**, 2133 (1963).
[38] H. Nifenecker, C. Signarbieux, R. Babinet, and J. Poitou, in *Proceedings of the Third International Atomic Energy Agency Symposium on the Physics and Chemistry of Fission, Rochester, 1973* (International Atomic Energy Agency, Vienna, 1974), p. 117.
[39] A. S. Vorobyev, V. N. Dushin, F.-J. Hambsch, V. A. Jakolev, V. A. Kalinin, A. B. Laptev, B. F. Petrov, and O. A. Shcherbakov, in *Proceedings of the International Conference on Nuclear Data for Science and Technology, ND2004, Santa Fe, 2004*, edited by R. C. Haight *et al.*, AIP Conf. Proc. No. 769 (AIP, Melville, New York, 2005).
[40] J. W. Boldeman, in *"Nuclear Data Standards for Nuclear Measurements,"* edited by H. Conde, Report No. NEANDC-311U, INDC(SEC)-101, 1991, p. 108.
[41] P. Santi and M. Miller, Nucl. Sci. Eng. **160**, 190 (2008).
[42] P. Talou, in *Proceedings of the International Workshop on Nuclear Fission and Fission Product Spectroscopy, Cadarache, France, 2009*, Ref. [16], p. 261.
[43] H. O. Denschlag, I. Tsekhanovich, M. Davi, F. Gönnenwein, M. Wöstheinrich, H. R. Faust, and S. Oberstedt, in *Proceedings of the 4th Seminar on Fission, Castle of Pont d'Oye, Habay-la Neuve, Belgium, 1999*, edited by C. Wagemans *et al.* (World Scientific, Singapore, 2000), p. 5.
[44] F. Gönnenwein (private communication).
[45] N. V. Kornilov, F.-J. Hambsch, and A. S. Votobyev, Nucl. Phys. A **789**, 55 (2007).
[46] K.-H. Schmidt and B. Jurado, Phys. Rev. Lett. **104**, 212501 (2010).
[47] W. Manhart, in IAEA Report No. IAEA-TECDOC-410, 1987, p. 158.
[48] J. Terrell, Phys. Rev. **113**, 527 (1959).
[49] F.-J. Hambsch, A. Tudora, G. Vladuca, and S. Oberstedt, Ann. Nucl. Energy **32**, 1032 (2005).
[50] H. Nifenecker, C. Signarbieux, M. Ribrag, J. Poitou, and J. Matuszek, Nucl. Phys. A **189**, 285 (1972).
[51] F. Gönnenwein, in *The Nuclear Fission Process*, Ref. [30], p. 287.
[52] J. Frehaut, in IAEA Report No. INDC(NDS)-220, 1989, p. 99.
[53] V. V. Verbinsky, H. Weber, and R. E. Sund, Phys. Rev. C **7**, 1173 (1973).
[54] E. Nardi, A. Gavron, and Z. Fraenkel, Phys. Rev. C **8**, 2293 (1973).
[55] R. Brun and F. Rademakers, Nucl. Instrum. Methods Phys. Res. Sect. A **389**, 81 (1997).